Probing the work generated by the autonomous rotation around a single ruthenium atom in an organometallic complex

Xun Li,[1‡] Yohan Gisbert,[2‡] Maxime Ledent,[1] Damien Sluysmans,[1] Gwénaël Rapenne,[2,3] Claire Kammerer,[2]* Anne-Sophie Duwez[1]*

[1] UR Molecular Systems, Department of Chemistry, University of Liège, Liège, Belgium

[2] CEMES, Université de Toulouse, CNRS, 29 rue Marvig, 31055 Toulouse, France

[3] Division of Materials Science, Nara Institute of Science and Technology, 8916-5 Takayama, Ikoma, Nara, Japan

[‡] These authors contributed equally

* Correspondence and requests for materials should be addressed to A.-S.D. (asduwez@uliege.be, force spectroscopy experiments) or C.K. (claire.kammerer@cemes.fr, synthesis)

Abstract

A variety of rotary molecular motors powered by light, chemical energy or tunnelling electrons have been synthesized and their operation in solution, in gels or on surfaces has been demonstrated. However, the single-molecule mechanics of such machines remain scarcely studied and very little data regarding their quantified performances have been disclosed. Here, we report on the synthesis of a series of molecules incorporating a five-arm rotor subunit and the direct quantitative measurement of the work generated by its rotation around the central ruthenium atom. We have used single-molecule force spectroscopy (SMFS) to detect the autonomous oscillations. We demonstrate that a mechanical load does not prevent rotation and show that the chemical nature of the arms influences the energy barrier, causing differences in the work that the motor can generate. Our results illustrate that SMFS, which is now widely used to probe processes at the scale of a few tens of nanometers in biomacromolecules, can detect motions around a single atom in a tiny synthetic molecule.

Introduction

Inspired by the molecular machinery of biological systems, chemists have developed a number of synthetic molecules that can perform tasks from translational or rotational motion when triggered by various external chemical or physical stimuli.[1–7] Based on diverse mechanically active synthetic units, artificial molecular machines exhibit a wide variety of functions such as muscles,[8–9] pumps,[10-14] transporters,[15] synthesizers,[16-21] molecular scissors,[22] elevators,[23] walkers, [24–25] nanovehicles,[26-28] and gears,[29-34] to name a few. In particular, rotary molecular motors have attracted much attention for their capacity to convert chemical, light or electric energy into a unidirectional rotation movement, leading to the production of work[1-7, 35-36] recoverable up to the macroscopic scale.[37-41] Controlled directional and repetitive rotation has been triggered on entire single molecules located in an anisotropic environment[42-45] or on submolecular fragments incorporated in diverse chemical architectures.[46-54]

In this context, an azimuthal molecular motor based on a ruthenium(II) piano-stool complex was proposed in 2013 and investigated on a Au(111) surface in ultra-high vacuum at the single-molecule scale.[42] The upper pentaarylcyclopentadienyl ligand acts as a five-arm rotor undergoing favoured

rotation over the ruthenium ion, which behaves as a single-atom pivot. The second ligand, a hydrotris(indazolyl)borate scorpionate, acts as a stator with a dual role: it lifts up the ruthenium ball-bearing from the surface thanks to its tripodal shape and, most importantly, it precludes molecular diffusion thanks to specific functionalization with three thioether groups allowing a tight anchoring on gold.[55] At low temperature (down to 5 K), when random thermal motion is suppressed, controlled rotation of the pentaarylcyclopentadienyl subunit is triggered by supplying electrical energy with a submolecular resolution using the tip of a Scanning Tunneling Microscope (STM). The resulting motion is unidirectional and reversibility has been evidenced, with a direction of rotation depending on the nature of the rotor fragment located under the STM tip during the inelastic electron tunneling process.[42] However, the drastic conditions of STM, namely ultra-high vacuum and low temperature conditions, limit potential applications. To accelerate the development of complex and automated machineries that can be operated on surfaces or in macroscopic materials,[6,38,40] it is desirable to investigate the behaviour of such motors in solution and ambient conditions. Furthermore, an important question like *can the motor still rotate when loaded*? remains unanswered.

Here, we used atomic force microscopy (AFM)-based single-molecule force spectroscopy (SMFS) to detect the autonomous rotation of the rotor subunit around a single ruthenium atom under mechanical load in molecular motor prototypes and directly probe at the single-molecule scale the work generated by such organometallic complexes. SMFS is now widely used to probe processes at the scale of a few tens of nanometers in biomacromolecules and has proved efficacious in deciphering mechanistic information of individual biomolecular machines and in quantifying their force response to external stress.[56-57] However, only a few investigations on intramolecular processes and single-molecule mechanics have been realized on small synthetic molecules, successful examples including molecular recognition pairing,[58] helical structures,[59] knots,[60] and artificial molecular machine prototypes.[61-66] The rarity of such studies stems from the difficulty in developing proper tools and preparing appropriate molecules that can be interfaced with SMFS techniques due to the very small amplitude of the involved motions compared the ones observed in previously studied larger biological systems or polymers, especially when probing conformational changes of synthetic small molecules interconverting between rotamers under Brownian fluctuations.

To this aim, new molecular motor prototypes based on ruthenium heteroleptic complexes were designed, so as to incorporate in the rotor subunit a long poly(ethylene oxide) (PEO) chain able to physisorb onto the AFM tip for pulling and monitoring rotor's movements. A series of molecules displaying structurally-different arms were synthesized and bridged between a gold substrate and a gold-coated AFM tip (Figure 1). The mechanical response of this series of motors bearing various rotor subunits was investigated and quantified in solution at room temperature.

Results and Discussion

Molecular design and synthesis

In anticipation of the SMFS studies, a new design of ruthenium-based molecular motor was devised by incorporating into the rotor subunit a long poly(ethylene oxide) chain (n=23, ~8 nm), able to physisorb onto the AFM tip (Figure 1). This polymer was connected to the central cyclopentadienyl ring via an amide moiety, selected for increased synthetic modularity, and a hydrocarbon spacer group such as a 4,4'-biphenyl fragment (**M1**). In order to study the influence of the spacer length and structure on the mechanical behaviour of the motor, one shorter 4-ethynylphenyl spacer (**M2**, **M3**) and one longer 4-

(biphenylethynyl)phenyl spacer (**M4**) were also designed. Finally, the four remaining substituents of the cyclopentadiene core were either kept identical to the previously-reported motor[42] using 4-ferrocenylphenyl groups (**M3**) or replaced with less hindered 4-bromophenyl moieties (**M1**, **M2**, **M4**). This family of four molecular motors incorporating a poly(ethylene oxide) chain (**M1**-**M4**) were prepared according to a common modular synthetic approach, relying on the post-functionalization of a 1,2,3,4,5-penta(*p*-halogenophenyl)cyclopentadienyl hydrotris(indazolyl) borate ruthenium(II) key precursor (compound **1**, scheme S1).[33] A single cross-coupling reaction under statistical[67] or chemoselective[68] conditions led respectively to the formation of the desired biphenyl or phenylethynyl pattern in the spacer group. Subsequent deprotection of the terminal benzylic or propargylic amine was followed by a condensation reaction with a monodisperse methoxy-PEG24-propionic acid partner, activated as an *N*-hydroxysuccinimidyl ester, to afford the target motors **M1**, **M2** and **M4**. In the case of motor **M3**, an extra four-fold Suzuki-Miyaura reaction was required as an intermediate step to install the four ferrocenyl moieties (see the SI section for detailed synthetic routes).[68]

Grafting onto surfaces

To provide stable attachment of the molecules on the substrates during SMFS measurements, each leg of the tripodal stator is anchored to the gold surface through a thioether group located on the 6-position of the indazole moiety (Figure 1). The molecules were grafted in solution onto gold-coated silicon substrates following the protocol reported previously to attain a low grafting density and favour single-molecule attachments with the tip[59–61] (see SI for details).

Rotation under mechanical load

During the force spectroscopy measurements, the AFM tip approaches the motor-functionalized substrate and interactions with the PEO tether are established (Figure 1). Then, increasing the distance between the tip and the surface, the force response of the molecule under extension is monitored by the deflection of the cantilever. Force-distance profiles were obtained for **M1** in *N*,*N*-dimethylformamide (DMF) at a pulling rate of 200 $nm.s^{-1}$. A characteristic and reproducible profile (Fig. 2a) with a discontinuity pattern that resembles a small tilted plateau was observed. This profile can be subdivided in three successive steps. First, the PEO tether is elongated and aligned in the pulling direction at low forces and distances, following the behaviour of a typical worm-like chain (WLC), an entropic elasticity model that predicts the relationship between the extension of a flexible polymer and its entropic restoring force (red trace).[69] At this stage of pulling, the external stress is not yet applied to the motor and its motion is not directly probed. Next, once the force value is close to the stall force of the rotor (*i.e*. the force value required to block its rotation), a different pattern appears on the force-distance profile, directly related to the motion of the rotor subunit in the ruthenium complex. Indeed, the arm being linked to the PEO tether is dragged in alignment with the pulling direction of the tip. It is important to note that the rotor initial position before the forceful alignment is completely random, due to non-directional oscillations around the ruthenium atom at room temperature. Thus, it leads to one oscillation with an angle up to 180 degrees, and therefore to the appearance of a pseudo-plateau in the force curve. The maximum length of this signal is related to the diameter of the rotor, and more precisely to the distance L (Figure 1) between the centre of the cyclopentadienyl core and the amide group attached to the PEO chain (see below and SI section IV.1). Once this last rotation has been performed and the attachment point of the PEO on the rotor is perfectly aligned with the pulling direction, the stretching of the PEO resumes following a second WLC profile (red trace) until the final detachment of the PEO

from the tip.

Histograms were built from force curves collected from different batches of experiments performed on different days (Figure 2b and c), giving the most probable values for the force (53 ± 19 pN) corresponding to the stall force of the motor, and length (1.8 ± 0.7 nm) of the characteristic small tilted plateau (Table 1). We find that the pseudo-plateau length measured is consistent with the theoretical length release for rotating half a turn. Indeed, if the molecule rotates during the pulling, the tension in the PEO tether decreases as a result of the length release. The maximum length release when rotating half a turn cannot be determined precisely. It is equal to the difference between the hypotenuse and the side of the right angle of the triangle made by the tip and the maximum diameter of the rotor (2 × L). This difference depends on the position of the tip with respect to the rotor. The theoretical maximum diameter of this rotor being 2.27 nm (Table 1, see SI section IV.1 for the details of the DFT calculations), the length release can be expected to extend between 0 and ~2 nm.

To test our hypothesis that the pseudo-plateau is indeed due to the rotation of the ligand around the ruthenium atom, we reproduced the same experiments on motors with spacers of different lengths (Figure 1 and S1-3). We found that the variation of the pseudo-plateau length is in strong correlation with the lengths of the functionalised arms (Table 1, Figures S1-3 and SI section IV.1). For **M2**, bearing a 4-ethynylphenyl linker (2 × L= 1.92 nm), we observed shorter lengths compared to **M1** (2 × L = 2.27 nm) and for **M4**, having a 4-(biphenylethynyl)phenyl moiety (2 × L = 3.64 nm), longer lengths. For **M3**, which is similar to **M2** but incorporates bulkier substituents as a control, no length variation occurred, as expected.

As a supplementary control experiment, we investigated the force response of a system (**M5**) where two side by side motors are linked chemically (Figure 3) to block the rotation. In this dinuclear ruthenium complex, the upper rotating subunit of the ruthenium complex **M1** is covalently linked via an alkyne moiety to the pentaarylcyclopentadienyl ligand of a second ruthenium complex. Upon adsorption of **M5** on gold via both thioether-appended tripods, motion of the rotor subunits is thus suppressed. This dinuclear complex was prepared according to a convergent synthetic route involving a key chemoselective Sonogashira coupling between two distinct half-sandwich ruthenium(II) complexes, such as the desymmetrized penta(*p*-halogenophenyl)cyclopentadienyl ruthenium(II) precursor **1b** and complex **14**, in which the cyclopentadienyl ligand bears a single ethynylphenyl substituent surrounded by four phenyl groups (Schemes S2 and S3). Introduction of the 4,4'-biphenyl spacer and of the PEO chain on the resulting dinuclear species **15** were next achieved according to the synthetic route detailed above for the preparation of motors **M1**-**M4** (see SI for details on the synthetic route). When motor **M5** was grafted on gold and studied by SMFS, no pseudo-plateau was detected in the force-distance profile (Figure S4). From these two control experiments, it is thus reasonable to attribute the pseudo-plateau to the stall force of rotation. We can thus conclude that we can detect the rotary motion of the rotor subunit around the ruthenium ion in motors **M1**-**M4** at room temperature and in a solution at the single molecule level. It is worth reminding here that these motors do not rotate unidirectionally at room temperature, but constantly oscillate non-directionally. What is detected with the tip are therefore the oscillations when they take place in the adequate direction to act on the AFM tip.

Pulling-relaxing experiments during which the molecule was stretched and relaxed for several cycles before detaching from the tip were also carried out. Figure 4 shows a representative pulling-relaxing force-extension curve in one cycle for motor **M1**. We observe that the pseudo-plateau also appears in the relaxing curves, while decreasing the tip–surface distance. This means that, as the force decreases and approaches the stall force value of the rotor, the latter is able to reinstate its rotation. This rotation

of the cyclopentadienyl ligand around the ruthenium atom appears as the typical plateau connecting both behaviours (the two WLC traces, Figure 2a), therefore observable on pulling and relaxing curves.

Rotation under various loading rates

We performed experiments on **M1** at different pulling rates to investigate the loading-rate dependency of the rotation. For experiments at 1000 $nm.s^{-1}$, pseudo-plateaus were also obtained (Figure S5), showing that the rotor subunit still rotates under a higher loading rate of 8000 $pN.s^{-1}$. When we decreased the pulling rate at 20 $nm.s^{-1}$ (160 $pN.s^{-1}$), we observed, surprisingly, a repeatable wave pattern (Figure 5a). Such a pattern is characteristic of force fluctuations between two states: one corresponding to the molecule exerting force on the AFM tip, the other one to the system in which tension is released. These fluctuations show that the motor is still able to rotate under the external load applied by the cantilever. When using a high pulling rate, the tip pulls too fast to detect the fluctuations and only the pseudo-plateau corresponding to the last rotation before the stoppage of the rotor is detected. The force at the end of the fluctuations observed with the pulling rate of 20 $nm.s^{-1}$ (~50 pN in Figure 5a) corresponds nicely to the force of the pseudo-plateau obtained for a higher pulling rate (53 ± 19 pN, Figure 2a and b).

From previous studies,[42] we know that this family of molecular motors oscillates constantly under ambient conditions and can be frozen only at a very low temperature, below 77 K. According to our SMFS results, the autonomous rotation time of **M1** is about 0.045 s per turn at room temperature (Figure S6. The total time from zero point to the end of fluctuations divided by the number of fluctuations equals the time for rotating one turn autonomously). When using a relatively high pulling rate, 200 $nm.s^{-1}$, the time allocated to the molecule to rotate under external force, 0.03 s, is lower than the autonomous rotation time (0.045 s). When using a slower pulling rate (20 $nm.s^{-1}$), the time allocated to the molecule to rotate during the pulling (0.3 s) is much longer than the autonomous rotation time (Figure S6), allowing several autonomous rotations before reaching the stall force.

The amplitude of the fluctuations (ΔF) represents the force that the molecule is able to exert against the pulling. The distribution (Figure 5b) shows that the molecule is able to exert a force of 14 pN on average (up to 40 pN), against an external load (Fapp) of up to 80 pN.

Influence of the nature of the rotor arms

To uncover the effect of the chemical structure of the rotor on its motion, we analysed the pseudo-plateau forces for the molecular motors bearing different arms (**M2**-**M4**, Figure 1). The pseudo-plateau force obtained for **M2**, bearing a phenylethynyl spacer instead of a 4,4'-biphenyl fragment, is centred around 62 ± 16 pN (Table 1). This means that the stall force of the rotating subunit of **M2** is higher than the force for **M1** (53 ± 19 pN), which is certainly due to a strong interplay between steric but also electronic factors. For **M3**, in which the spacer is identical to **M2** but the bromine atom on each arm is replaced by a ferrocenyl group, we observe a higher pseudo-plateau force (74 ± 15pN). The force increase between **M2** and **M3**, bearing identical linkers, can be largely explained by a higher steric hindrance between the rotor and stator, due to the presence of the ferrocenyl moieties in **M3** (Table 1). Indeed, a higher steric hindrance induces a higher energy barrier for the rotation and thus the possibility to generate a higher mechanical work against the pulling when rotation takes place. An increase in the steric interactions between both ligands in the ruthenium complex thus results in an increase of the force required to block the rotation. Finally, for **M4** incorporating four *p*-bromophenyl groups on the rotor, the measured pseudo-plateau force is around 66 ± 23 pN, similar to **M2**. Although the spacers are

different in **M2** and **M4**, they both display a phenylethynyl fragment directly connected to the central cyclopentadienyl core. The peripheral biphenyl part of **M4** is too far away from the rotation axis to cause any steric interactions with the stator or have a major electronic effect. This elongated spacer does not change the intrinsic barrier of rotation for **M4**, leading to the same pseudo-plateau forces for **M2** and **M4**. Motors **M1**-**M4** thus follow the same rotating mode and present the same type of pseudo-plateau pattern in pulling curves, while the stall force depends on the steric hindrance between rotor and stator as a major parameter.

As mentioned above, the autonomous rotation can be observed when the pulling rate is low enough. We observed pulling curves with repeatable fluctuations for each molecule for a pulling rate of 20 $nm.s^{-1}$, similar to what has been observed for **M1**. Representative curves are shown in Figure S7.

We also extrapolated the rotation time of **M2**-**M4** at room temperature and results are shown in Figure S8. We notice that the rotation time of this series of motors are similar at room temperature, 0.045 s per turn, which corresponds to a speed of 1333 turns per minute, even for **M3** with larger steric hindrance and **M4** with a longer spacer. These results show that temperature is probably the most vital effect on controlling the speed of autonomous rotational motion, rather than the chemical structure and length of the arms for this series of rotors.

Work performed by the motors

In order to evaluate the mechanical work that these ruthenium-centred molecular motors can generate, we measured the integrated area below the last fluctuation (from point B to A, Figure 5a) and between the two WLC fits as the maximum work performed by the rotor against the mechanical load. The mechanical work output of the motors is summarized in Table 2. The work produced by **M1** and **M2** is about 13-15 k_BT (~ 8 $kcal.mol^{-1}$) and is higher (25-30 k_BT, ~ 15 $kcal.mol^{-1}$) for **M3** and **M4**, due to a higher force for **M3** and a higher rotor diameter for **M4**.

The power output was deduced from these data, by dividing the work by the duration of a single rotation (Table 2). The power output is centred at about 3.10^{-18} W for motors **M1** and **M2** and at about $5\text{-}6.10^{-18}$ W for their counterparts **M3** and **M4**.

Conclusion

We have designed, synthesized and probed a series of single-molecule motors based on a piano-stool ruthenium complex that differ by the chemical nature and length of their arms. The results of the SMFS investigations show that we can detect the autonomous rotation of the rotor subunit around a single atom and quantify the force response to external stress. They also show that the motors can still rotate when they are loaded. The stall force varies between ~50 and 70 pN, as a result of an interplay between electronic and steric effects. When the mechanical load is increased well beyond the motor stall force, the rotor can reinstate its rotation as soon as the load is decreased down to the stall force. The work generated by these motors, between ~13 and 30 k_BT, also depends on the chemical structure and length of the rotors' arms. On the basis of a measured rotation time of 0.045 s per turn and the work output, we determined a power output in the order of 10^{-18} W for this series of molecular motors.

More generally, the study shows the very first example of detecting and quantifying motions around a single atom by single-molecule force spectroscopy, and illustrates the utility that this technique can offer for evidencing details of the molecular design that are crucial for improved efficiency and applicability of synthetic molecular machines.

SUPPLEMENTARY INFORMATION

The supplementary information can be found at:

ACKNOWLEDGMENTS

This work was supported by the European Union's Horizon 2020 research and innovation programme under the project MEMO, grant agreement No 766864, the JSPS KAKENHI Grant-in-Aid for Challenging Research (20K21131), and the F.R.S.-FNRS (GEQ U.G017.22 and EQP U.N032.18). DFT calculations were performed using HPC resources from CALMIP (Grant 2020-p20041). The University Toulouse 3-Paul Sabatier (Toulouse) and NAIST are also thanked for providing a crossed position to G.R. Y.G. thanks the French Ministry of National Education for a PhD Fellowship. D.S. is a Postdoctoral Researcher of the F.R.S.-FNRS (Chargé de recherches).

AUTHOR CONTRIBUTIONS

A.-S.D., G.R. and C.K. designed the experiments. Y.G. carried out the chemical synthesis and characterization studies. X.L. and M.L. performed the AFM experiments and X.L. and D.S. analyzed the data. A.-S.D., G.R. and C.K. directed the research. All the authors discussed the results and commented on the manuscript.

DECLARATION OF INTERESTS

The authors declare no competing interests.

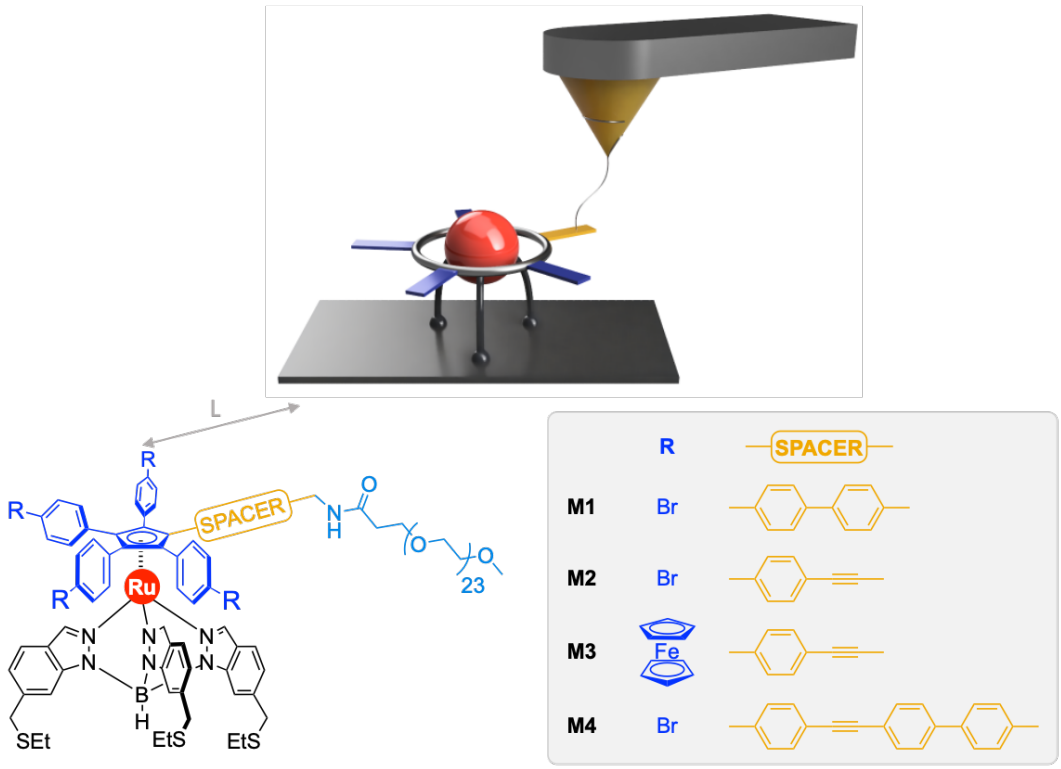

Figure 1. Schematics of the SMFS experiment and molecular structures of the motors **M1**-**M4**.

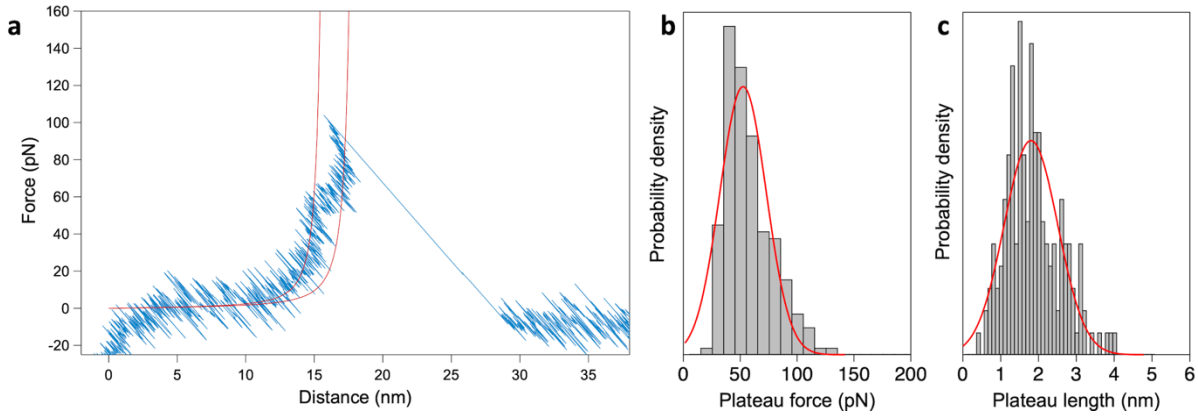

Figure 2. **a.** Characteristic force-distance profile obtained for **M1** at a pulling rate of 200 nm.s^{-1}. Two worm-like chain (WLC) fits are added in red as a guide to the eye (before and after the pseudo-plateau). **b**. Histogram of the pseudo-plateau force (red trace: Gaussian Fit). *N*=200. **c**. Histogram of the pseudo-plateau length (red trace: Gaussian Fit). *N*=200.

Table 1. Pseudo-plateau length and force for **M1**-**M4** at a pulling rate of 200 nm.s^{-1} Most probable values (± s.d.) obtained from the fitting of the distribution of the raw data with Gaussian functions. *N*=200 for **M1**, *N*=174 for **M2**, *N*=337 for **M3**, *N*=354 for **M4**. The maximum rotor diameters (2 × L) have been obtained from DFT calculations (see details in SI section IV.1).

	M1	M2	M3	M4
Pseudo-plateau length (nm)	1.8 ± 0.7	1.3 ± 0.5	1.3 ± 0.5	2.2 ± 1.0
Pseudo-plateau force (pN)	53 ± 19	62 ± 16	74 ± 15	66 ± 23
Maximum rotor diameter (nm)	2.27	1.92	1.92	3.64

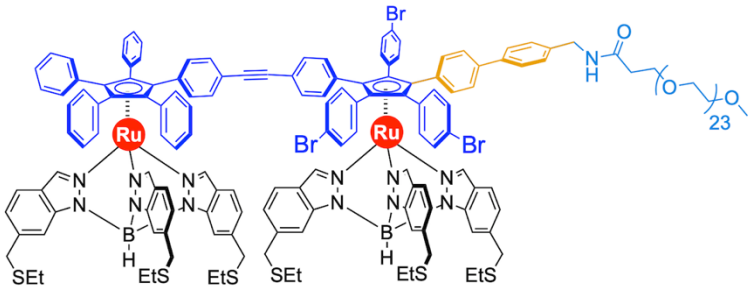

Figure 3. Molecular structure of the system **M5** in which two side by side motors are linked chemically to block the rotation.

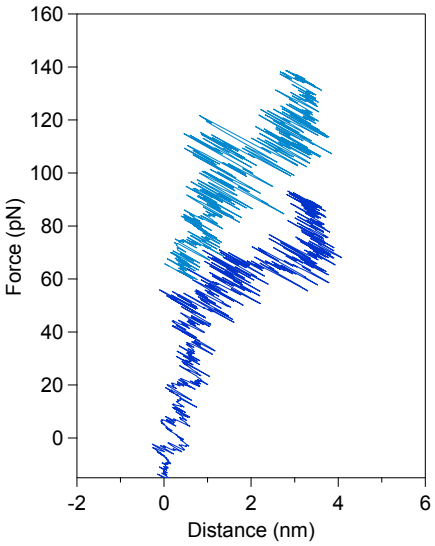

Figure 4. Characteristic pulling (light blue)–relaxing (dark blue) force-extension cycle obtained for **M1** at a pulling rate of 200 nm.s^{-1} The pulling trace is offset vertically for clarity.

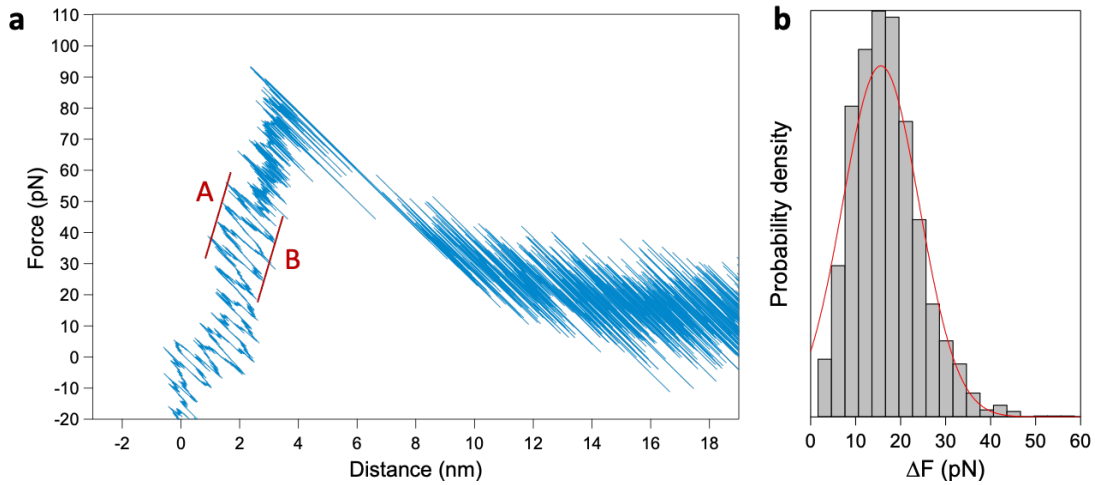

Figure 5. **a**. Characteristic force-distance profile obtained for **M1** at a pulling rate of 20 nm.s^{-1}. **b**. Histogram of the amplitude of the fluctuations (ΔF) (red trace: Gaussian Fit). N=1681.

Table 2. Work and power output for **M1**-**M4**. Most probable values (± s.d.) obtained from the fitting of the distribution of data with Gaussian functions. *N*=94 for **M1**, *N*=115 for **M2**, *N*=121 for **M3**, *N*=103 for **M4**.

	M1	M2	M3	M4
Work output (k_BT)	15.3 ± 7.8	13.6 ± 5.0	29.6 ± 12.8	24.7 ± 12.6
Power output (10^{-18} W)	3.2 ± 1.7	2.8 ± 1.0	6.2 ± 2.7	5.0 ± 2.6

References

1. Special issue on molecular motors: see Iino, R., Kinbara, K. & Bryant, Z. Introduction: Molecular Motors. *Chem. Rev.* 120, 1-4 (2020).
2. Coskun, A., Banaszak, M., Astumian, R. D., Stoddart, J. F. & Grzybowski, B. A. Great expectations: can artificial molecular machines deliver on their promise? *Chem. Soc. Rev*. 41, 19–30 (2012).
3. Guix, M., Mayorga-Martinez, C. C. & Merkoçi, A. Nano/micromotors in (bio)chemical science applications. *Chem. Rev*. 114, 6285–6322 (2014).
4. Erbas-Cakmak, S., Leigh, D. A., McTernan, C. T. & Nussbaumer, A. L. Artificial molecular machines. *Chem. Rev*. 115, 10081–10206 (2015).
5. Kassem, S., van Leeuwen, T., Lubbe, A. S., Wilson, M. R., Feringa, B. & Leigh, D. A. Artificial molecular motors. *Chem. Soc. Rev*. 46, 2592-2621 (2017).
6. Krause, S. & Feringa, B. L. Towards artificial molecular factories from framework-embedded molecular machines. *Nat. Rev. Chem.* 4, 550–562 (2020).
7. Borsley, S., Leigh, D. A. & Roberts, B. M. W. Chemical fuels for molecular machinery. *Nat. Chem*. 445, 728–738 (2022).
8. Jiménez, M. C., Dietrich-Buchecker, C. & Sauvage, J.-P. Towards Synthetic Molecular Muscles: Contraction and Stretching of a Linear Rotaxane Dimer. *Angew. Chem. Int. Ed.* 39, 3284–3287 (2000).
9. Bruns, C. J. & Stoddart, J. F. Rotaxane–based molecular muscles. *Acc. Chem. Res*. 47, 2186—2199 (2014).
10. Serreli, V., Lee, C.-F., Kay, E. R. & Leigh, D. A. A molecular information ratchet. *Nature* 445, 523–527 (2007).
11. Ragazzon, G., Baroncini, M., Silvi, S., Venturi, M. & Credi, A. Light-powered autonomous and directional molecular motion of a dissipative self-assembling system. *Nat. Nanotechnol.* 10, 70–75 (2014).
12. Cheng, C., McGonigal, P. R., Schneebeli, S. T., Li, H., Vermeulen, N. A., Ke, C. & Stoddart, J. F. An artificial molecular pump. *Nat. Nanotechnol*. 10, 547–553 (2015).
13. Amano, S., Fielden, S. D. P. & Leigh, D. A. A catalysis-driven artificial molecular pump. *Nature* 594, 529–534 (2021).
14. Thomas, D., Tetlow, D. J., Ren, Y., Kassem, S., Karaca, U. & Leigh, D. A. Pumping between phases with a pulsed-fuel molecular ratchet. *Nat. Nanotechnol.* 17, 701–707 (2022).
15. Kassem, S., Lee, A. T. L., Leigh, D. A., Markevicius, A. & Solà, J. Pick-up, transport and release of a molecular cargo using a small-molecule robotic arm. *Nat. Chem*. 8, 138–143 (2016).

16. Thordarson, P., Bijsterveld, E. J. A., Rowan, A. E. & Nolte, R. J. M. Epoxidation of polybutadiene by a topologically linked catalyst. *Nature* 424, 915–918 (2003).
17. Lewandowski, B., De Bo, G., Ward, J. W., Papmeyer, M., Kuschel, S., Aldegunde, M. J., Gramlich, P. M. E., Heckmann, D., Goldup, S. M., D'Souza, D. M., Fernandes, A. E. & Leigh, D. A. Sequence-specific peptide synthesis by an artificial small-molecule machine. *Science* 339, 189–193 (2013).
18. Kassem, S., Lee, A. T. L., Leigh, D. A., Marcos, V., Palmer, L. I. & Pisano, S. Stereodivergent synthesis with a programmable molecular machine. *Nature* 549, 374-378 (2017).
19. De Bo, G., Gall, M. A. Y., Kuschel, S., De Winter, J., Gerbaux, P. & Leigh, D. A. An artificial molecular machine that builds an asymmetric catalyst. *Nat. Nanotechnol.* 13, 381-385 (2018).
20. McTernan, C., De Bo, G. & Leigh, D. A. A track-based molecular synthesizer that builds a single-sequence oligomer through iterative carbon-carbon bond formation. *Chem* 6, 2964-2973 (2020).
21. Heard, A. W., Meijide Suárez, J. & Goldup, S. M. Controlling catalyst activity, chemoselectivity and stereoselectivity with the mechanical bond. *Nat. Rev. Chem*. 6, 182, (2022).
22. Muraoka, T., Kinbara, K., Kobayashi, Y. & Aida, T. Light-Driven Open–Close Motion of Chiral Molecular Scissors. *J. Am. Chem. Soc.* 125, 5612–5613 (2003).
23. Badjić, J. D., Balzani, V., Credi, A., Silvi, S. & Stoddart, J. F. A Molecular Elevator. *Science* 303, 1845–1849 (2004).
24. von Delius, M., Geertsema, E. M. & Leigh, D. A. A synthetic small molecule that can walk down a track. *Nat. Chem*. 2, 96–101 (2010).
25. Leigh, D. A., Lewandowska, U., Lewandowski, B. & Wilson, M. R. Synthetic molecular walkers. *Top. Curr. Chem*. 354, 111-138 (2014).
26. Kudernac, T., Ruangsupapichat, N., Parschau, M., Maciá, B., Katsonis, N., Harutyunyan, S. R., Ernst K.-H. & Feringa, B. L. Electrically driven directional motion of a four-wheeled molecule on a metal surface. *Nature* 479, 208–211 (2011).
27. Nishino, T., Martin, C. J., Takeuchi, H., Lim, F., Yasuhara, K., Gisbert, Y., Abid, S., Saffon-Merceron, N., Kammerer, C. & Rapenne, G. Dipolar Nanocars Based on a Porphyrin Backbone. *Chem. Eur. J.* 26, 12010–12018 (2020).
28. Simpson, G. J., García-López, V., Petermeier, P., Grill, L. & Tour, J. M. How to build and race a fast nanocar. *Nat. Nanotechnol.* 12, 604–606 (2017).
29. Ube, H., Yasuda, Y., Sato, H. & Shionoya, M. Metal-centred azaphosphatriptycene gear with a photo- and thermally driven mechanical switching function based on coordination isomerism. *Nat. Commun.* 8, 14296 (2017).
30. Frantz, D. K., Linden, A., Baldridge, K. K. & Siegel, J. S. Molecular Spur Gears Comprising Triptycene Rotators and Bibenzimidazole-Based Stators. *J. Am. Chem. Soc.* 134, 1528–1535 (2012).
31. Au Yeung, K. H., Kühne, T., Eisenhut, F., Kleinwächter, M., Gisbert, Y., Robles, R., Lorente, N., Cuniberti, G., Joachim, C., Rapenne, G., Kammerer, C. & Moresco, F. Transmitting Stepwise Rotation among Three Molecule-Gear on the Au(111) Surface. *J. Phys. Chem. Lett.* 11, 6892–6899 (2020).
32. Gisbert, Y., Abid, S., Kammerer, C. & Rapenne, G. Molecular Gears: From Solution to Surfaces. *Chem. Eur. J.* 27, 12019–12031 (2021).
33. Abid, S., Gisbert, Y., Kojima, M., Saffon-Merceron, N., Cuny, J., Kammerer, C. & Rapenne, G. Desymmetrised pentaporphyrinic gears mounted on metallo-organic anchors. *Chem. Sci.* 12, 4709–4721 (2021).
34. Gerwien, A., Gnannt, F., Mayer, P. & Dube, H. Photogearing as a concept for translation of precise motions at the nanoscale. *Nat. Chem.* 14, 670–676 (2022).

35. Bach, N. N., Josef, V., Maid, H. & Dube, H. Active Mechanical Threading by a Molecular Motor. *Angew. Chem. Int. Ed.* 61, e202201882 (2022).
36. Kathan, M., Crespi, S., Troncossi, A., Stindt, C. N., Toyoda, R. & Feringa, B. L. The Influence of Strain on the Rotation of an Artificial Molecular Motor. *Angew. Chem. Int. Ed.* 61, e202205801 (2022).
37. Eelkema,R., Pollard, M. M., Vicario, J., Katsonis, N., Serrano Ramon, B., Bastiaansen, C. W. M., Broer, D. J. & Feringa, B. L. Nanomotor rotates microscale objects. *Nature* 440, 163 (2006).
38. Li, Q., Fuks, G., Moulin, E., Maaloum, M., Rawiso, M., Kulic, I., Foy, J. T. & Giuseppone, N. Macroscopic contraction of a gel induced by the integrated motion of light-driven molecular motors. *Nat. Nanotechnol*. 10, 161–165 (2015).
39. Foy, J. T., Li, Q., Goujon, A., Colard-Itté, J.-R., Fuks, G., Moulin, E., Schiffmann, O., Dattler, D., Funeriu, D. P. & Giuseppone, N. Dual-light control of nanomachines that integrate motor and modulator subunits. *Nat. Nanotechnol*. 12, 540–545 (2017).
40. Moulin, E., Faour, L., Carmona-Vargas, C. C. & Giuseppone, N. From Molecular Machines to Stimuli-Responsive Materials. *Adv. Mater*., 32, 1906036 (2020).
41. Moulin, E., Faour, L., Carmona-Vargas, C. C. & Giuseppone, N. Extraction of mechanical work from stimuli-responsive molecular systems and materials. *Trends in Chemistry*, 3, 926–942 (2021).
42. Perera, U. G. E., Ample, F., Kersell, H., Zhang, Y., Vives, G., Echeverria, J., Grisolia, M., Rapenne, G., Joachim C. & Hla, S.-W. Controlled clockwise and anticlockwise rotational switching of a molecular motor. *Nat. Nanotechnol*. 8, 46–51 (2013).
43. Simpson, G. J., García-López, V., Daniel Boese, A., Tour, J. M. & Grill, L. How to control single-molecule rotation. *Nat. Commun.* 10, 4631 (2019).
44. Zhang, Y., Calupitan, J. P., Rojas, T., Tumbleson, R., Erbland, G., Kammerer, C., Ajayi, T. M., Wang, S., Curtiss, L. A., Ngo, A. T., Ulloa, S. E., Rapenne, G. & Hla, S. W. A chiral molecular propeller designed for unidirectional rotations on a surface. *Nat. Commun.* 10, 3742 (2019).
45. Stolz, S., Gröning, O., Prinz, J., Brune, H. & Widmer, R. Molecular motor crossing the frontier of classical to quantum tunneling motion. *Proc. Natl. Acad. Sci. USA* 117, 14838–14842 (2020).
46. Koumura, N., Zijlstra, R. W. J., van Delden, R. A., Harada, N. & Feringa, B. L. Light-driven monodirectional molecular rotor. *Nature* 401, 152–155 (1999).
47. Leigh, D. A., Wong, J. K. Y., Dehez, F. & Zerbetto, F. Unidirectional rotation in a mechanically interlocked molecular rotor. *Nature* 424, 174–179 (2003).
48. Hernández, J. V., Kay, E. R. & Leigh, D. A. A reversible synthetic rotary molecular motor. *Science* 306, 1532–1537 (2004).
49. Fletcher, S. P., Dumur, F., Pollard, M. M. & Feringa, B. L. A reversible, unidirectional molecular rotary motor driven by chemical energy. *Science* 310, 80–82 (2005).
50. Greb, L. & Lehn, J.-M. Light-driven molecular motors: imines as four-step or two-step unidirectional rotors. *J. Am. Chem. Soc*. 136, 13114–13117 (2014).
51. Wilson, M. R., Solà, J., Carlone, A., Goldup, S. M., Lebrasseur, N. & Leigh, D. A. An autonomous chemically fuelled small-molecule motor. *Nature* 534, 235–240 (2016).
52. Gerwien, A., Mayer, P. & Dube, H. Green light powered molecular state motor enabling eight-shaped unidirectional rotation. *Nat. Commun.* 10, 4449 (2019).
53. Mo, K., Zhang, Y., Dong, Z., Yang, Y., Ma, X., Feringa, B. L. & Zhao, D. Intrinsically unidirectional chemically fuelled rotary molecular motors. *Nature* 609, 293–298 (2022).
54. Borsley, S., Kreidt, E., Leigh, D. A. & Roberts, B. M. W. Autonomous fuelled directional rotation about a covalent single bond. *Nature* 604, 80–85 (2022).

55. Kammerer, C. & Rapenne, G. Scorpionate hydrotris(indazolyl)borate ligands as tripodal platforms for surface-mounted molecular gears and motors. *Eur. J. Inorg. Chem*. 2214–2226 (2016).
56. Duwez, A.-S. & Willet, N. (2012). Molecular Manipulation with Atomic Force Microscopy (CRC Press).
57. Müller, D. J., Dumitru, A. C., Giudice, C. L., Gaub, H. E., Hinterdorfer, P., Hummer, G., De Yoreo, J. J., Dufrêne, Y. F. & Alsteens, D. Atomic force microscopy-based force spectroscopy and multiparametric imaging of biomolecular and cellular systems. *Chem. Rev*. 121, 11701–11725 (2021).
58. Sluysmans, D., Zhang, L., Li, X., Garci, A., Stoddart, J. F. & Duwez, A.-S. Viologen tweezers to probe the force of individual donor-acceptor π-interactions. *J. Am. Chem. Soc*. 142, 21153–21159 (2020).
59. Devaux, F., Li, X., Sluysmans, D., Maurizot, V., Bakalis, E., Zerbetto, F., Huc, I. & Duwez, A.-S. Single-molecule mechanics of synthetic aromatic amide helices: ultrafast and robust non-dissipative winding. *Chem* 7, 1333–1346 (2021).
60. Calvaresi, M., Duwez, A.-S., Leigh, D. A., Sluysmans, D., Song, Y., Zerbetto, F. & Zhang, L. Mechanical tightening of a synthetic molecular knot. *Chem* 9, 65–75 (2023).
61. Lussis, P., Svaldo-Lanero, T., Bertocco, A., Fustin, C.-A., Leigh, D. A. & Duwez, A.-S. A single synthetic small molecule that generates force against a load. *Nat. Nanotechnol*. 6, 553–557 (2011).
62. van Quaethem, A., Lussis, P., Leigh, D. A., Duwez, A.-S. & Fustin, C.-A. Probing the mobility of catenane rings in single molecules. *Chem. Sci.* 5, 1449–1452 (2014).
63. Naranjo, T., Lemishko, K. M., de Lorenzo, S., Somoza, A., Ritort, F., Perez, E. & Ibarra, B. Dynamics of individual molecular shuttles under mechanical force. *Nat. Commun*. 9, 4512 (2018).
64. Sluysmans, D., Hubert, S., Bruns, C. J., Zhu, Z., Stoddart, J. F. & Duwez, A.-S. Synthetic oligorotaxanes exert high forces when folding under mechanical load. *Nat. Nanotechnol*. 13, 209–213 (2018).
65. Sluysmans, D., Devaux, F., Bruns, C. J., Stoddart, J. F. & Duwez, A.-S. Dynamic force spectroscopy of synthetic oligorotaxane foldamers. *Proc. Natl. Acad. Sci. USA* 115, 9362–9366 (2018).
66. Sluysmans, D., Lussis, P., Fustin, C.-A., Bertocco, A., Leigh, D. A. & Duwez, A.-S. Real-time fluctuations in single- molecule rotaxane experiments reveal an intermediate weak binding state during shuttling. *J. Am. Chem. Soc*. 143, 2348–2352 (2021).
67. Gisbert, Y., Kammerer, C. & Rapenne, G. Divergent synthesis of molecular winch prototypes. *Chem. Eur. J*. 27, 16242–16249 (2021).
68. Gisbert, Y., Abid, S., Bertrand, G., Saffon-Merceron, N., Kammerer, C. & Rapenne, G. Modular synthesis of pentaarylcyclopentadienyl Ru-based molecular machines via sequential Pd-catalysed cross couplings. *Chem. Commun*. 55, 14689–14692 (2019).
69. Flory, P. J. Statistical Mechanics of Chain Molecules (Hanser, 1989).